ELSEVIER

Cement & Concrete Composites 26 (2004) 127–140

Cement & Concrete Composites

www.elsevier.com/locate/cemconcomp

Limit capacity of laterally restrained reinforced concrete floor slabs in fire

A.S. Usmani *, N.J.K. Cameron

School of Engineering and Electronics, University of Edinburgh, Edinburgh EH9 3JN, UK

Accepted 25 April 2003

Abstract

This paper presents a new concept for determining the limit capacity of rectangular reinforced concrete slab panels subjected to fire. The results from extensive previous work on computational modelling of composite steel frame structures in fire at the University of Edinburgh has shown that the response of such structures is dominated by the thermal strains induced in the structure as a result of heating. Naturally, as the limit state of collapse is approached, the conventional influences of loading and structural strength and stiffness (reduced by heating) will once again begin to dominate the response. However, in tests carried out on such structures and in many instances of real fires no collapse or failure has been observed and the exact mechanism of failure is still a matter for speculation. Because of this apparently considerable robustness of composite framed structures in fire, tests (such as the full scale fire tests at Cardington) have been carried out (with fire protection applied to the steel columns only while most steel beams being left unprotected), but again without any structural failure. A number of investigations, including the authors own, have attributed this robustness to the tensile membrane mechanism in the composite deck slab. The research group at Edinburgh has discovered that the development of tensile membrane mechanism in fire is much more reliable relative to ambient conditions. This is because the large amount of thermal strain allows composite floor systems to assume highly deflected shapes while limiting the magnitude of damaging tensile mechanical strains, thereby retaining the ability to carry loads for much longer. In the context of performance based design this additional capacity of composite decks or reinforced concrete slabs can be exploited for providing structural stability in fire given that a quantitative estimate of this capacity can be reliably made. Some previous work exists in this regard but none of this work attempts to determine the correct deflected geometry of the floors and therefore the membrane capacity is not properly estimated. This paper introduces a new three-step method that analyses the limit capacity of laterally restrained RC slabs in fire. First the temperature distribution over the depth of the slab is estimated for a given fire scenario. Then the deflected shape of the RC slab and its membrane stress state is determined using a rigorous analytical method. Finally an energy based method is used to determine the maximum load that the slab could carry based on the geometric form and stress state determined in the previous steps.

Keywords: Laterally restrained RC slabs in fire; Thermal expansion; Thermal bowing; Large deflections; Limit capacity

1. Introduction

Over the last decade a great deal of new knowledge has been generated towards understanding the behaviour of structures in fire. This is particularly true for composite steel framed structures with concrete deck floor systems. The impetus for this accelerated development was initially provided by the Broadgate fire [1], followed by the full scale fire tests at BRE's Large Building Test Facility (LBTF) at Cardington [2]. An extensive program of computational modelling of the Cardington tests led by University of Edinburgh, in collaboration with British Steel (now Corus), Imperial College, BRE and SCI [3] under the sponsorship of DETR 'Partners in Technology' scheme. The findings from this work have been reported extensively [4–7]. The details of modelling and subsequent interpretations of behaviour are too voluminous to present here, but considerable information can be downloaded from the web page given in [3]. Very briefly, this work revealed

* Corresponding author. Address: School of Civil and Environmental Engineering, University of Edinburgh, Crew Building, The King's Buildings, Edinburgh EH9 3JN, Scotland, UK. Tel.: +44-131-650-5789; fax: +44-131-650-6781.

E-mail address: asif.usmani@ed.ac.uk (A.S. Usmani).

0958-9465/$ - see front matter © 2003 Elsevier Ltd. All rights reserved.
doi:10.1016/S0958-9465(03)00090-8

Nomenclature

$D = Eh^3/12(1-v^2)$	flexural stiffness of plate
h	thickness of plate
F	Airy stress function
B, L	plate dimensions
E	Young's modulus
v	Poisson's ratio
α	coefficient of thermal expansion
ΔT	thermal expansion
$T_{,z}$	thermal gradient
M^{T}	thermal moment
N^{T}	thermal force
w_{T}	deflection due to thermal load
w_{q}	deflection due to ultimate load
w_{t}	total deflection
q_{ult}	ultimate load
$\sigma_{\mathrm{y},T}$	yield stress in rebar at temperature T
Π_{ext}	external work done by load
Π_{int}	internal work done by reinforcement
ϵ_{uk}	strain limit at maximum load
$\sigma_{w_{\mathrm{T}}}$	mechanical stress due to thermal deflection
$\epsilon_{w_{\mathrm{T}}}$	mechanical strain due to thermal deflection
$\sigma_{w_{\mathrm{t}}}$	mechanical stress due to total deflection
$\epsilon_{w_{\mathrm{t}}}$	mechanical strain due to total deflection

the following lessons for whole structure behaviour in fire:

- Restraint to thermal strain dominates the structural behaviour (in terms of internal forces and displacements).
- Relative to thermal strains, the contribution of conventional (gravity) loading is low (if no failure occurs).
- The results show low sensitivity to variations in strength and stiffness properties of steel, as thermal expansion swamps these effects.
- At large deflections, tensile membrane action in the spans and compressive membrane action near the perimeter supports of floor slabs are observed.
- Thermal strains automatically produce a beneficial load-carrying shape for tensile membrane action in slabs, without large and damaging mechanical strains
- The load capacity is further enhanced by thermally induced pre-stressing in laterally restrained slabs and composite floor systems.
- Local buckling of the lower flanges of steel beams (acting compositely with the slab) occurs quite at relatively low steel temperatures (between 100 and 200 °C) but this was not found to be a detrimental mechanism.

A number of generally applicable fundamental principles of structural behaviour in fire were identified as part of the modelling and analysis exercise [7]. For instance, a simple analysis will reveal that in composite structural members restrained from lateral translation at the supports (but free to rotate), as the mean temperature increases, compression occurs, but as the through-depth temperature gradient increases, tension occurs. The former scenario is most likely in a slow growing, protracted fire, while the latter may result from a rapidly growing, short duration fire. The understanding developed in this manner led the authors to investigate the possibility of developing new design methods for floor systems in fire which may be used in a performance based design, as more and more building codes are beginning to accept this as an alternative to prescriptive methods.

The Cardington fire tests and subsequent modelling work has shown that tensile membrane action in the floor system is the final resisting mechanism in a building fire before collapse. This fact is implicitly recognised by a number of authors [8,9] and they have proposed methods to enable quantification of the load carrying capacity at the fire limit state. The work of Bailey and Moore [9,10] in particular provides a detailed method which has led to the publication of a design guide by SCI [11]. Whereas these methods are of considerable practical benefit, they do not account for the correct shape of the floor system under the influence of heating. This is because these methods develop previous work [12,13] quantifying the enhancement to load carrying capacity by membrane effects, but for ambient conditions. Therefore, in effect they extend the ambient temperature failure shapes based on flexural failure (yield line mechanism) to apply to the fire situation. It can be shown that at the fire limit state the bending resistance of slabs is practically negligible and the eventual failure will not occur in the manner of a yield line failure (which is essentially a low-deflection mechanism). The correct slab deflected shape (with very large deflections) resulting from accommodating the large thermal strains (extension and curvature) provides much enhanced membrane capacity. As this becomes the dominant load carrying mechanism well before failure, it is therefore reasonable to assume that failure will be initiated by tensile yield and rupture of reinforcement (most likely at the supports, where the maximum membrane tensions occur). This scenario is entirely different from yield line theory assumptions, where (for slabs free to rotate at boundaries) failure is initiated by yielding in the mid-span regions (where maximum bending moments occur).

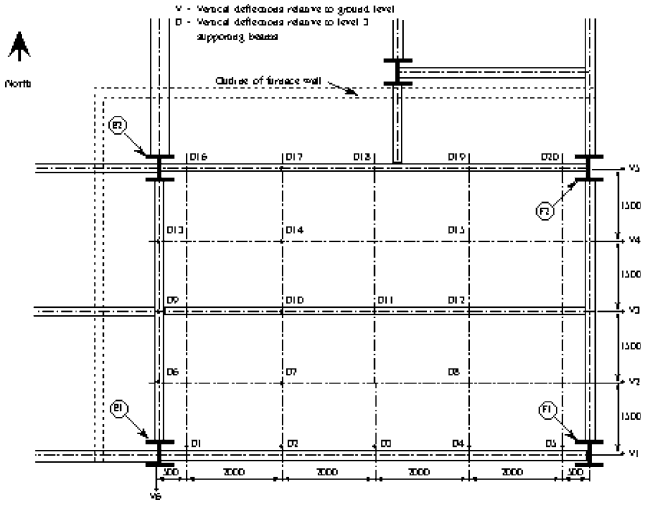

Fig. 1. The layout of British Steel Corner test at Cardington, with deflection measurement locations.

Incorporating the correct deflected shape and failure mechanism to quantify the membrane capacity in fire conditions requires several new developments. The first is to develop a reliable estimate of the temperature distribution in the reinforced concrete floor slab, followed by determining the correct deflected shape and the ultimate load carrying capacity based on an assumed failure mechanism. Fig. 1 shows the structural layout and the fire compartment boundaries for the British Steel Corner Test at Cardington with deflection measurement locations. Fig. 2 shows the actual deflected shape of the slab at 80 min, which corresponds to the peak atmosphere temperature in the fire compartment. Fig. 3 shows the deflected shape at 100 min, which corresponds to the peak deflection (and by implication the highest mean temperature in the slab), this is as expected [7]. This indicates that the slab temperature distribution dominates the deflected shape and the unprotected steel beams have a considerably lower influence (see Fig. 1), because between 80 and 100 min the unprotected beams are cooling (while the deflection continues to increase). The extraordinary smoothness of the deflected shapes themselves indicates this (no impression of the grid of secondary beams underneath appears). The fire protected columns and edge beams are much stiffer and the slab is clearly seen to 'drape' over them (a full analysis of this test appears in [5]). The highly curved form of the deflected slab with a maximum deflection of about 400 mm suggests that it is highly unlikely that any classical yield line failure patterns could occur.

The deflected shape is governed by the temperature distribution in the slab and consequent generalised thermal strains (mean thermal expansion and curvature) [7], with negligible contribution from the reinforcement. The ultimate membrane capacity clearly is governed by the residual capacity of the reinforcement and its anchorage at the compartment boundaries. To estimate the residual capacity the stress state of the reinforcement is required. Depending upon the slab temperature distribution and boundary restraint conditions, the reinforcement can be either in compression (in which case extra membrane capacity is available) or in tension (with reduced capacity) [7,14]. The new concepts presented here account for all of these conditions and the following sections provide details of these developments.

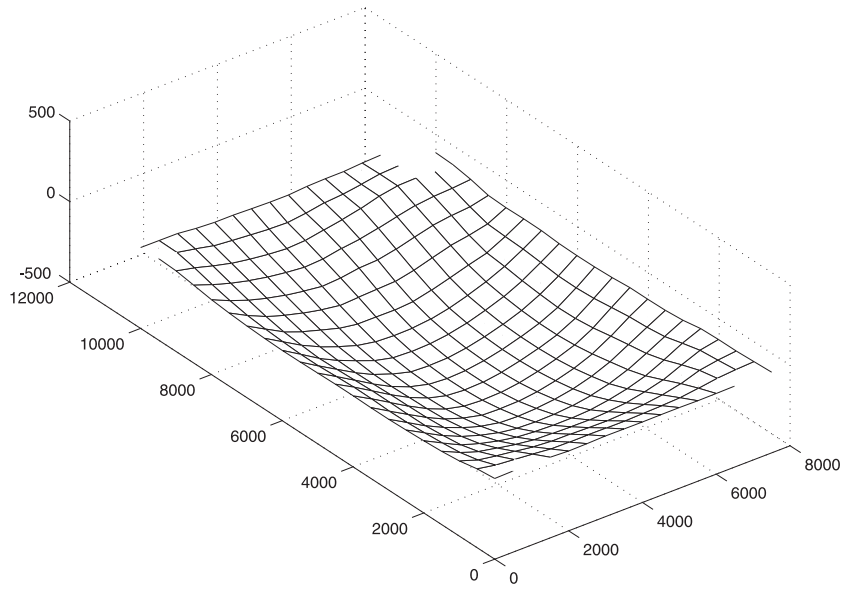

Fig. 2. Measured Corner Test deflections at 80 min: at peak fire temperature.

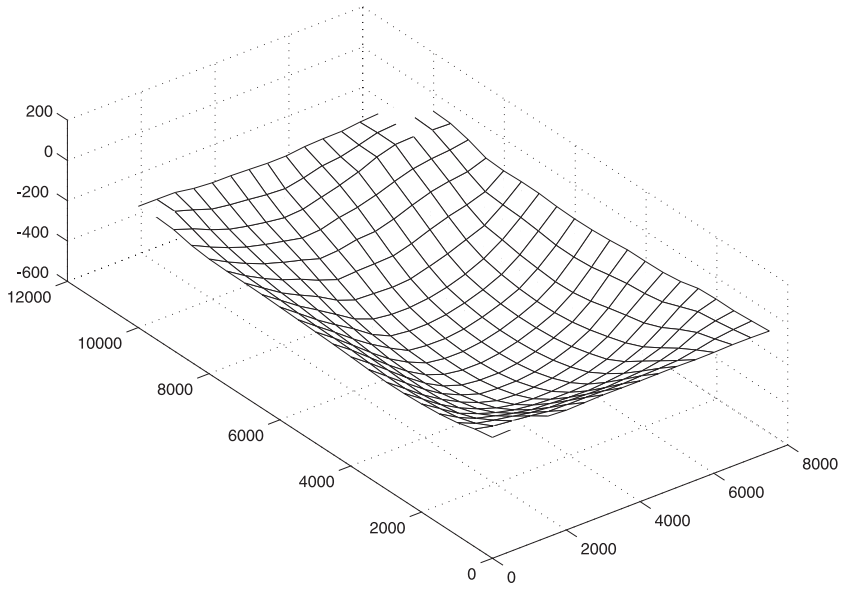

Fig. 3. Measured Corner Test deflections at 100 min: at peak slab deflection.

2. Analysis procedure

The analysis procedure is based on a number of simplifying assumptions based on the authors understanding of floor panel behaviour in fire. Fig. 4 shows a schematic of a corner compartment for reference. The assumptions are:

(1) The slab is assumed to be rectangular in plan.

(2) The slab is assumed to be restrained against lateral translation (translation in the original plane of the slab) at all boundaries and free to rotate about the axes coincident with each boundary. This is a reasonable assumption as very little restraint to lateral translation is actually required for slender members [7], as slabs

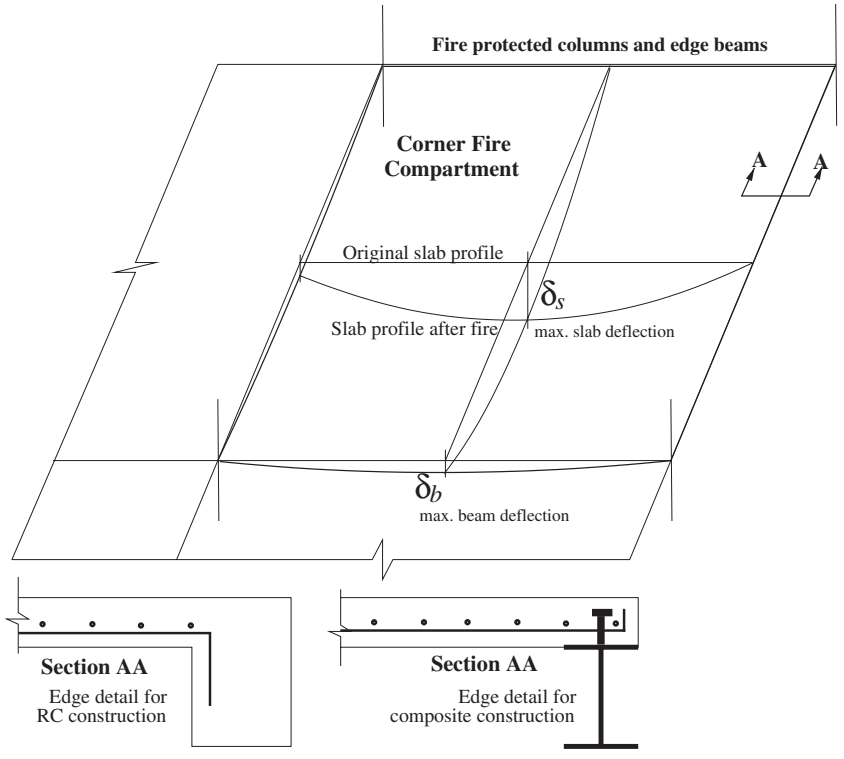

Fig. 4. Schematic of a corner fire compartment after the fire.

indeed are. Thermal gradients apply large 'hogging' (negative) moments at supports if rotations are restrained. If there is no reinforcement against these moments at the supports, rotations will freely occur (away from the stiff corners).

(3) Anchorage to tensile membrane forces in the slab is available at the perimeter. To enable reliable tensile membrane mechanism, it is necessary that the floor slab reinforcement is anchored at the compartment perimeter. While interior continuity may reliably be provided by lapping of reinforcement, edge and corner compartments have discontinuous edges and will only provide the required restraint if edge beams are fire protected and the reinforcement is anchored to the edge beams in some fashion (suggested detailing shown in Fig. 4). In addition to the detailing, this assumption is further helped by the development of compressive membrane behaviour in the slab along the perimeter supports (because of restrained thermal expansion without large deflections and also from the geometric size difference of the slab and the clear distance between supports—this phenomenon also occurs at ambient temperatures, referred to as a 'compression ring' [8]).

(4) Temperature distribution in the slab varies only through the depth of the slab (i.e. $T = f(z)$ and $(\partial T/\partial x) = (\partial T/\partial y) = 0$).

(5) The material behaviour for both concrete and steel is considered temperature dependent and uniaxial properties based on EC2 and EC3 are used. The EC properties are further simplified as elastic perfectly plastic with infinite ductility unless a rupture strain is specified. This assumption is reasonable based on high temperature properties of steel and concrete.

(6) The failure during the heating phase of the fire is assumed to occur in a ductile manner (runaway) and no localisation of strain occurs in the reinforcement. This, coupled with the previous assumption, observations from Cardington tests and the modelling work is again a reasonable assumption. There is evidence of localised strains and reinforcement rupture over the supports in the Cardington tests [9], however the authors modelling work [3] suggests that this did not occur during the heating regime. Modelling of the cooling regime was not undertaken. However, simple analysis suggests that the tensions caused during cooling may be sufficient to fracture reinforcement at several locations over the supports (not unlike the commonly observed fracture of steel connections). This paper presents a method for calculating the load capacity during the heating phase of the fire only.

(7) The fire limit state is assumed to have reached when any part of the reinforcement achieves a mechanical strain equal to a conservative estimate of the rupture strain (for instance 2.5% for cold rolled steel reinforcement).

(8) At this stage the effect of beams is not considered and the compartment perimeter beams are assumed to deflect much less than the centre of the slab ($\delta_b \ll \delta_S$).

(9) The deflected shape is entirely governed by the temperature distribution in the slab.

(10) Tensile membrane capacity is derived entirely from the reinforcement.

(11) Reinforcement temperature is identical to the surrounding concrete and so is its thermal expansion coefficient (no slippage).

The proposed analysis is carried out in three stages described as follows:

(1) *Thermal input:* Determine the likely fire scenario (unless given), and calculate the temperature distribution over the depth ($T(z)$). Determine the equivalent thermal expansion ΔT and equivalent thermal gradient $T_{,z}$ of the whole slab or for each of the specified number of planar slices of the slab.

(2) *Mechanical response:* Determine the deflection profile of the reference surface of the slab ($w(x,y)$) for the given temperature distribution and the associated stress and strain states at the reference surface ($\sigma(x,y)$) and $\epsilon(x,y)$ (coincident with the plane of reinforcement).

(3) *Load capacity:* Determine ultimate membrane capacity using an energy method.

Each of the above procedures require a considerable amount of effort. To provide a clear and detailed description, each step is separately discussed in the following sections.

3. Thermal input

One of the key conclusions from the research so far is that structural response to fire depends upon the rate of heating as well as the temperature of the structure, and that different fires can produce very different stress/strain patterns in composite floor systems [3]. This is because most of the pre-failure response of structural members depends upon the two geometric effects produced by heating, a mean temperature increase and a mean thermal gradient [7]. The material effects of reduction in strength and stiffness with temperature increase also require accurate estimates of the temperature distribution. The following subsections discuss the three main parts of this exercise.

3.1. Fire scenario

The fire scenario can be obtained using a number of different approaches. The simplest of these will be to adopt one of a number of standard fires, i.e. BS476 or ASTME119. If however the details of the fire compartment are known (or can be estimated as part of design data, including geometry, ventilation and thermal characteristics of the wall linings and fuel load) then a better approach is to use a natural fire. This can be

based on Eurocode 1 parametric relationships [15] (as chosen here) or any other suitable method.

3.2. Temperature distribution over slab depth

The temperature distribution over the depth of the slab can be calculated using a numerical procedure. This can be done using the analytical solution [16] for 1D heat conduction accounting for heat absorption due to evaporation phase change for the free water and the water of hydration in the concrete. This solution however does not account for temperature dependency of the thermal properties in concrete and other nonlinearities [6]. Therefore, a 1D finite element program was written to calculate the temperature distribution. Exposition of this work is outside the scope of this paper, however for general details of finite elements for heat transfer, refer to [17]. The program developed was applied to 100 mm thick lightweight concrete slab subjected to a Eurocode 1 parametric fire. The fuel load was assumed to be 750 MJ/m^2, the opening factor was 0.08 $m^{\frac{1}{2}}$ and the thermal inertia of the wall lining was 1100 J m^2 s$^{\frac{1}{2}}$K. Fig. 5 shows the variation of temperature over the depth of the slab at various times during the fire scenario, both during the heating and cooling phases (before and after peak fire temperature).

3.3. Estimation of equivalent temperature effects on the model

Given that the cross-sections of composite structural members and the temperature distributions over their depths can be quite complicated, the issue of equivalent thermal loading that must be applied to the members is not straightforward. A procedure has been developed based upon ideas used in estimating the effects of thermally induced stresses in bridge decks [18] and described in [19]. Using this procedure any temperature distribution over the depth of any structural section can be represented by an equivalent mean temperature and mean thermal gradient. This procedure is applied to the 100 mm lightweight concrete slab subjected to the fire specified earlier. Fig. 6(a) shows various temperatures against time (including the mean slab temperature). Fig. 6(b) shows the equivalent temperature gradient variation over time.

4. Determination of the deflection profile and stress state as a result of the fire

The change in the temperature distribution in a slab due to a fire will cause a thermal load to act on the slab. Due to this load the slab will deflect resulting in a change in the stress and strain distribution within the slab. The total load on the slab can therefore be considered to consist of two components; the normal design load, consisting of the dead and applied loads, and the thermal load. Both loads must be considered when designing a slab to resist fire. The design method presented in this paper separates the two loads and considers them individually. In this section a method is presented for determining the deflection of a slab and the resulting stress and strain distribution due to the thermal loading only. The dead and applied loads are considered in Section 5 when determining the ultimate load capacity of the slab.

In obtaining the solution for the deflection profile and stress–strain distribution in a slab due to a thermal load

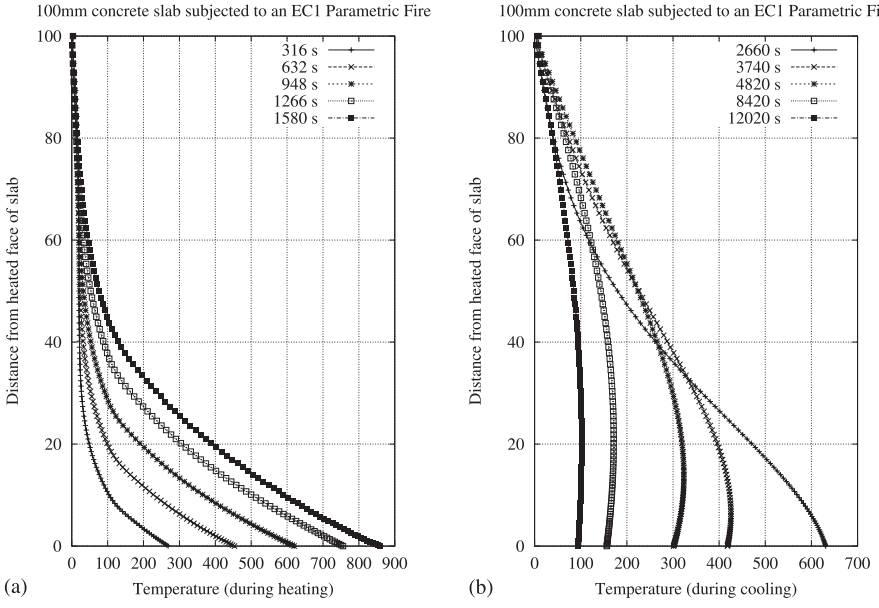

Fig. 5. Temperature distribution in the slab over the whole fire scenario: (a) heating and (b) cooling phase.

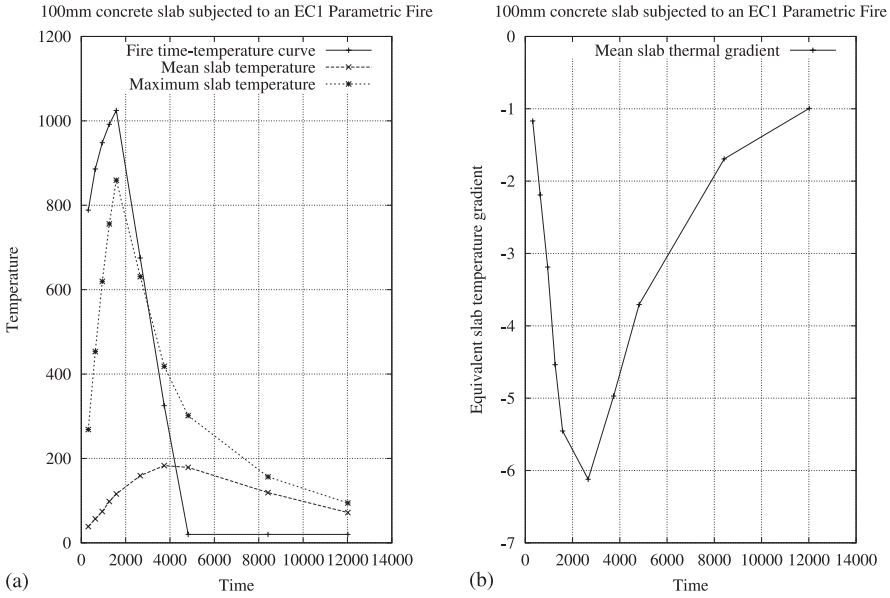

Fig. 6. Time variation of temperatures and equivalent thermal gradient over slab depth: (a) mean temperatures and (b) equivalent slab temperature gradient.

two approximations were made. Finding an exact solution to the governing differential equations is very difficult as the membrane forces vary with both x and y. Using an Airy stress function allows a solution to be obtained, however, in doing so the result is that σ_{xx} can only vary in y and σ_{yy} can only vary in x. Secondly, the analysis is geometrically nonlinear, however, the material behaviour is linear i.e. material degradation is not considered. Although material softening does play an important role in the behaviour of a structure in a fire, its importance is not as great as traditionally thought. At the start of a fire the behaviour is governed by the thermal forces induced by restraint effects and the effects of material softening do not become evident until the structure nears failure. In the analysis method presented in this paper when calculating the deflection and stress state due to thermal loads it is assumed that the material is linear, however, when determining the ultimate load the effects of material property variation of the steel reinforcement are considered.

4.1. Thermal loading

The thermal loading is caused by the bending induced by the thermal gradient $T_{,z}$ and restraint to the thermal expansion ΔT. These cause a thermal moment M^{T} and a thermal force N^{T} respectively which can be calculated:

$$M^{\mathrm{T}} = E\alpha \int_{-h/2}^{h/2} T(z) z \, \mathrm{d}z = E\alpha T_{,z} \frac{h^3}{12} \tag{1}$$

$$N^{\mathrm{T}} = E\alpha \int_{-h/2}^{h/2} T(z) \, \mathrm{d}z = Eh\alpha\Delta T \tag{2}$$

4.2. Governing equations

To calculate the distribution of membrane stresses within a slab subjected to thermal loading there are two governing differential equations which must be solved. For stresses under large deflections to be obtained it is necessary to retain the nonlinear terms. The two equations to be solved are the equilibrium equation and the compatibility equation [20] which, for an isotropic flat slab subject to thermal loading, can be written as,

$$D\left(\frac{\partial^4 w}{\partial x^4} + 2\frac{\partial^4 w}{\partial x^2 y^2} + \frac{\partial^4 w}{\partial y^4}\right) - h\left(\frac{\partial^2 F}{\partial y^2}\frac{\partial^2 w}{\partial x^2} + \frac{\partial^2 F}{\partial x^2}\frac{\partial^2 w}{\partial y^2} - 2\frac{\partial^2 F}{\partial x \partial y}\frac{\partial^2 w}{\partial x \partial y}\right) + \frac{1}{1-v}\left(\frac{\partial^2 M^{\mathrm{T}}}{\partial x^2} + \frac{\partial^2 M^{\mathrm{T}}}{\partial y^2}\right) = 0 \tag{3}$$

$$h\left(\frac{\partial^4 F}{\partial x^4} + 2\frac{\partial^4 F}{\partial x^2 y^2} + \frac{\partial^4 F}{\partial y^4}\right) - Eh\left[\left(\frac{\partial^2 w}{\partial x \partial y}\right)^2 - \frac{\partial^2 w}{\partial x^2}\frac{\partial^2 w}{\partial y^2}\right] + \frac{\partial^2 N^{\mathrm{T}}}{\partial x^2} + \frac{\partial^2 N^{\mathrm{T}}}{\partial y^2} = 0 \tag{4}$$

where w is the deflection function for the slab, F is the Airy stress function, E is the Young's modulus, v is the Poisson's ratio, D is the flexural rigidity of the slab, M^{T} is the thermal moment and N^{T} is the thermal force.

4.3. Boundary conditions

Fig. 7 shows the slab to be analysed. The slab is assumed to be laterally restrained against translation but free to rotate along all four boundaries such that at $x = 0$ and L:

$$w = 0 \quad u = 0 \quad M_x = 0 \tag{5}$$

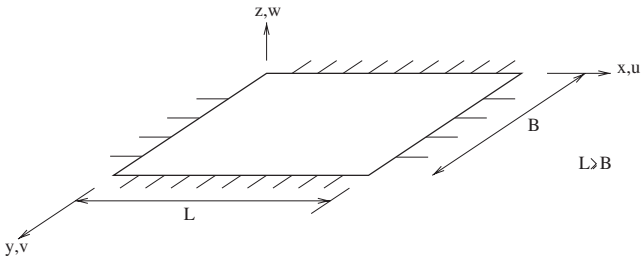

Fig. 7. Slab geometry.

and at $y = 0$ and $y = B$:

$$w = 0 \quad v = 0 \quad M_y = 0 \tag{6}$$

where u and v are the membrane displacements in the x and y directions respectively.

4.4. Solution for a slab subject to thermal loading

In obtaining a solution to the governing differential equations it is necessary to represent the deflection of the slab and the thermal moment as double Fourier series.

$$w(x,y) = \sum_{m=1}^{\infty}\sum_{n=1}^{\infty} w_{mn} \sin\frac{m\pi x}{L} \sin\frac{n\pi y}{B} \tag{7}$$

$$M^{\mathrm{T}}(x,y) = \sum_{m=1}^{\infty}\sum_{n=1}^{\infty} M^{\mathrm{T}}_{mn} \sin\frac{m\pi x}{L} \sin\frac{n\pi y}{B} \tag{8}$$

The Fourier coefficients M^{T}_{mn} are calculated by performing the Fourier integration:

$$M^{\mathrm{T}}_{mn} = \frac{4}{LB}\int_0^L \int_0^B M^{\mathrm{T}} \sin\frac{m\pi x}{L} \sin\frac{n\pi y}{B}\,\mathrm{d}x\,\mathrm{d}y \tag{9}$$

$$= \frac{16M^{\mathrm{T}}}{\pi^2 mn} \tag{10}$$

The thermal moment Fourier series can therefore be written as:

$$M^{\mathrm{T}}(x,y) = \sum_{m=1}^{\infty}\sum_{n=1}^{\infty} \frac{16M^{\mathrm{T}}_{mn}}{\pi^2 mn} \sin\frac{m\pi x}{L} \sin\frac{n\pi y}{B} \tag{11}$$

Considering only the first term in the series and substituting Eq. (7) into that for compatibility, Eq. (4), results in:

$$\frac{1}{E}\left(\frac{\partial^4 F}{\partial x^4} + 2\frac{\partial^4 F}{\partial x^2 y^2} + \frac{\partial^4 F}{\partial y^4}\right) = \frac{w_{11}^2\pi^4}{2L^2B^2}\left(\cos\frac{2\pi x}{L} + \cos\frac{2\pi y}{B}\right) \tag{12}$$

The general solution of the Airy stress function F consists of two parts, a homogeneous solution F_{H} and a particular solution F_{P}. The particular solution F_{P} is obtained by solving Eq. (12) such that:

$$F_{\mathrm{P}} = \frac{w_{11}^2 E}{32}\left(\frac{L^2}{B^2}\cos\frac{2\pi x}{L} + \frac{B^2}{L^2}\cos\frac{2\pi y}{B}\right) \tag{13}$$

The general solution of Eq. (4) can be described as:

$$F = P\frac{x^2}{2} + Q\frac{y^2}{2} + \frac{w_{11}^2 E}{32}\left(\frac{L^2}{B^2}\cos\frac{2\pi x}{L} + \frac{B^2}{L^2}\cos\frac{2\pi y}{B}\right) \tag{14}$$

For this analysis it was assumed that the plate was laterally restrained along all of its edges and that the elongations in the x and y directions were independent of y and x respectively. Considering this statement the values of P and Q can be calculated to be:

$$P = \frac{w_{11}^2\pi^2 E}{8(1-v^2)}\left(\frac{1}{B^2} + v\frac{1}{L^2}\right) - \frac{E\alpha\Delta T}{1-v}$$

$$Q = \frac{w_{11}^2\pi^2 E}{8(1-v^2)}\left(\frac{1}{L^2} + v\frac{1}{B^2}\right) - \frac{E\alpha\Delta T}{1-v}$$

The final solution for the Airy stress function F satisfying the equation of compatibility Eq. (4) can therefore be written as,

$$F = \frac{w_{11}^2\pi^2 E}{8(1-v^2)}\left(\frac{1}{B^2} + v\frac{1}{L^2}\right)\frac{x^2}{2} + \frac{w_{11}^2\pi^2 E}{8(1-v^2)}\left(\frac{1}{L^2} + v\frac{1}{B^2}\right)\frac{y^2}{2} + \frac{w_{11}^2 E}{32}\left(\frac{L^2}{B^2}\cos\frac{2\pi x}{L} + \frac{B^2}{L^2}\cos\frac{2\pi y}{B}\right) - \frac{E\alpha\Delta T}{1-v}\frac{x^2}{2} - \frac{E\alpha\Delta T}{1-v}\frac{y^2}{2} \tag{15}$$

By substituting Eqs. (7), (11) and (15) into the equation for equilibrium Eq. (3) and applying a Galerkin procedure [21] a cubic equation with respect to the deflection w_{11} of the plate is obtained. Defining the deflection caused by the thermal loading as w_{T} then the solution is:

$$\left\{\frac{1}{16}\pi^4 hE(3-v^2)\left[\frac{B}{L^3} + \frac{L}{B^3}\right] + \frac{1}{4LB}\pi^4 hEv\right\}w_{11}^3 + \left\{\pi^4 D(1-v^2)\left[\frac{B}{L^3} + 2\frac{1}{BL} + \frac{L}{B^3}\right] - \pi^2 hE\alpha\Delta T(1+v)\left[\frac{B}{L} + \frac{L}{B}\right]\right\}w_{11} - 16M^{\mathrm{T}}(1+v)\left[\frac{B}{L} + \frac{L}{B}\right] = 0 \tag{16}$$

Rearranging the above equation and defining the deflection due to the thermal loading as w_{T} then the solution is:

$$\frac{3}{4}\left\{(3-v^2)\left(1 + \frac{L^4}{B^4}\right) + 4v\frac{L^2}{B^2}\right\}\left(\frac{w_{\mathrm{T}}}{h}\right)^3 + \left\{\left(1 + \frac{L^2}{B^2}\right)^2 - 12\frac{L^2(1+v)N^{\mathrm{T}}}{\pi^2 Eh^3}\left(1 + \frac{L^2}{B^2}\right)\right\}\left(\frac{w_{\mathrm{T}}}{h}\right) - 192\frac{L^2(1+v)M^{\mathrm{T}}}{\pi^4 Eh^4}\left(1 + \frac{L^2}{B^2}\right) = 0 \tag{17}$$

Using the above equation the deflection w_T due to the fire can be determined. For a negative gradient it will produce a negative deflection. It can be seen from Eq. (17) that for a slab that has a thermal load, if the Young's modulus does not change through the depth, then the actual value of E does not affect the deflection as in every term of the equation it disappears (recall that E was used previously to calculate the thermal moment and thermal force). In an actual fire a portion of the slabs depth on the fire affected side would lose some of its strength, however, most of the slab would remain at its ambient strength. Therefore, although it is an approximation, it is felt that the above materially linear equation does provide a reasonable method of calculating the deflection of the slab due to a thermal load. Under the action of a normal design load the value of E does affect the deflection of the slab and it is, therefore, important that this is taken into account. In Section 5, which considers the effects of the normal design load, changing material properties due to the fire are considered.

4.5. Calculation of stress–strain distribution due to thermal loading

For a slab subjected to heating the total strain consists of two components; mechanical strain, $\epsilon_{\text{mechanical}}$, and thermal strain, $\epsilon_{\text{thermal}} = \alpha\Delta T$.

$$\epsilon_{\text{total}} = \epsilon_{\text{mechanical}} + \epsilon_{\text{thermal}} \tag{18}$$

The total strain ϵ_{total} is governed by the deflection of the slab, however, not all of this strain is converted into mechanical stress. Whether the stress state in the slab is elastic or plastic is governed by the mechanical strains. The effect of these thermal strains is that they allow the slab to develop the large deflections necessary to transmit load through tensile membrane action without having large mechanical strains. In comparison to a similar deflection under ambient conditions the mechanical strains in the reinforcement will be much lower and the slab will retain a much larger capacity for carrying load.

The membrane stress distribution along the boundary of the slab for any deflection w can be calculated using the Airy stress function in Eq. (15):

$$\sigma_{xx} = \frac{\partial^2 F}{\partial y^2} = \frac{w^2\pi^2 E}{8(1-v^2)}\left(\frac{1}{L^2} + \frac{v}{B^2}\right) - \frac{w^2\pi^2 E}{8L^2}\cos\frac{2\pi y}{B} - \frac{E\alpha\Delta T}{1-v} \tag{19}$$

$$\sigma_{yy} = \frac{\partial^2 F}{\partial x^2} = \frac{w^2\pi^2 E}{8(1-v^2)}\left(\frac{1}{B^2} + \frac{v}{L^2}\right) - \frac{w^2\pi^2 E}{8B^2}\cos\frac{2\pi x}{L} - \frac{E\alpha\Delta T}{1-v} \tag{20}$$

These equations can be used to determine the stress in a slab due to a deflection w. In this instance we are interested in the stress in the reinforcement so the Young's modulus should be that of the steel E_s.

Eqs. (19) and (20) can be rearranged to provide the mechanical membrane strains:

$$\epsilon_{xx,\text{mech}} = \frac{w^2\pi^2}{8L^2}\left(1 - \cos\frac{2\pi y}{B}\right) + v\frac{w^2\pi^2}{8B^2} - \alpha\Delta T \tag{21}$$

$$\epsilon_{yy,\text{mech}} = \frac{w^2\pi^2}{8B^2}\left(1 - \cos\frac{2\pi x}{L}\right) + v\frac{w^2\pi^2}{8L^2} - \alpha\Delta T \tag{22}$$

By removing the thermal components the total membrane strains can be calculated:

$$\epsilon_{xx,\text{total}} = \frac{w^2\pi^2}{8L^2}\left(1 - \cos\frac{2\pi y}{B}\right) + v\frac{w^2\pi^2}{8B^2} \tag{23}$$

$$\epsilon_{yy,\text{total}} = \frac{w^2\pi^2}{8B^2}\left(1 - \cos\frac{2\pi x}{L}\right) + v\frac{w^2\pi^2}{8L^2} \tag{24}$$

The values of x and y chosen should correspond to the positions of the reinforcement along the edge so that a mechanical stress and mechanical strain can be calculated for each bar. These will be defined as σ_{w_T}, ϵ_{w_T}. Should the calculated mechanical stress be greater than the yield stress then it is necessary to define the stress as $\sigma_{w_T} = \sigma_{y,T}$ where $\sigma_{y,T}$ is the yield stress of the reinforcement at a temperature T.

4.6. Analysis example

Using the method presented a 5 m × 5 m slab was analysed. The slab depth was 100 mm with a Young's modulus (E) of 40,000 N/mm^2 and a Poisson's ratio (v) of 0.3. Temperature distribution based on Section 3.2 causing an equivalent thermal gradient of $T_{,z} = 5$ °C/mm and an equivalent thermal expansion of $\Delta T = 200$ °C was chosen. This caused a thermal loading with a thermal moment (M^T) of 133 kN mm and a thermal force (N^T) of 6.4 kN. Results were compared against an analysis using the ABAQUS finite element package. Using Eq. (17) the deflection was calculated to be 148 mm. This compared well with the value of 136 mm from the finite element analysis. Eqs. (19), (21) and (23) were used to calculate the stress and strain distributions along the slab boundary. Fig. 8 shows the calculated membrane stresses along half of the length of the slab boundary in comparison with those obtained from the finite element analysis. It can be seen that the predicted results using the method derived previously agree with those predicted by the finite element analysis and show compression near the corners and tension near the middle of the edge. This agrees with the expected membrane distribution along the slab boundaries (see Fig. 10). The total and mechanical membrane strains along the slab boundary are shown in Fig. 9.

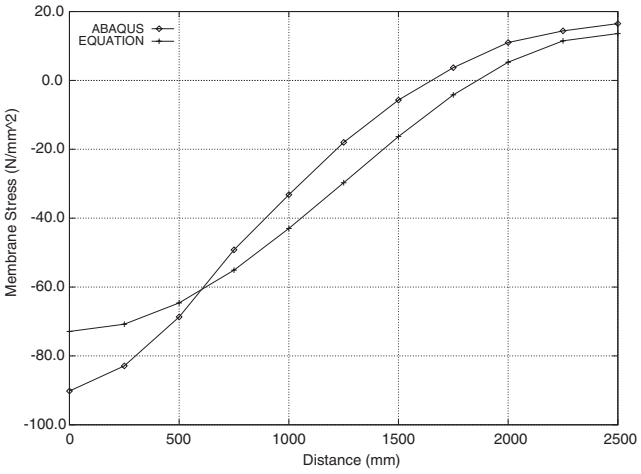

Fig. 8. Membrane mechanical stress distribution along slab boundary.

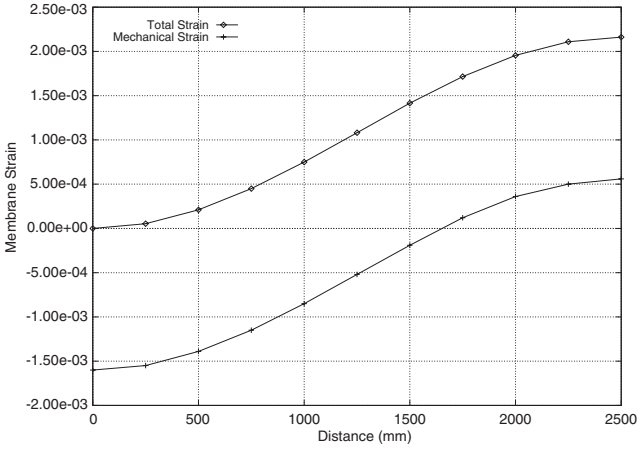

Fig. 9. Membrane strain distributions along slab boundary.

5. Determination of the ultimate membrane capacity

5.1. Design philosophy

Having determined the displacement, stress and strain of the slab due to thermal loading the ultimate load capacity of the slab can be calculated using an energy method. In doing so a number of conservative assumptions are made. It will be assumed that all of the load is carried through the membrane action of the slab thus ignoring any strength from the bending stiffness of the slab. Any tensile strength in the concrete will also be ignored so that all of the load is being carried by the reinforcing bars. Strain hardening of the reinforcement is ignored.

The total deflection of the slab w_t will be considered to consist of two components; the deflection caused by the thermal load, w_T, and the deflection caused by the design load, w_q, such that,

$$w_t = w_T + w_q \tag{25}$$

From the previous stage in the analysis a value for w_T has been calculated. It will be assumed that failure has been reached based on a limiting value for the mechanical strain in the reinforcement. Based on this value the total deflection w_t, at which point the slab is said to have reached failure, can be calculated. It is therefore possible to calculate w_q. The ultimate load (q_{ult}) will be calculated by equating the change in internal and external work done as the slab moves through the deflection w_q.

5.2. Failure criterion

To obtain a value for the ultimate load it is necessary to define a point at which failure is said to have been reached. Geometrical limits such as *span*/30 should not be applied in a situation such as this where, due to thermal expansion, large deflections do not necessarily mean the structure is near failure. A better approach is to apply a limiting value for the mechanical strain based on the ductility of the reinforcing bars. EC2 [22] recognises two classes of ductility, high ductility (H) and normal ductility (N). Table 1 shows the ductility properties given in EC2 where ϵ_{uk} is the characteristic value of the elongation at maximum load. EC2 states that reinforcement with a bar size of 16 mm or above can be treated as being highly ductile whereas if the bar size is 12 mm or less then normal ductility should be assumed.

For the purposes of this design method it will be assumed that the ultimate load has been reached when any of the reinforcing bars reaches this mechanical strain limit. In practice this will always occur in the reinforcing bars at the centre of the slab across the shortest span over supports. This is where the greatest tensile stresses occur. The total strain ϵ_{total} at which this point is reached is calculated by considering the ductility class and the thermal expansion such that:

$$\epsilon_{total} = \epsilon_{uk} + \alpha\Delta T \tag{26}$$

The limiting deflection w_t at which this total strain value is reached can be calculated using Eq. (22) as the shortest span will reach the mechanical yield strain limit first. By setting $\epsilon_{mech} = \epsilon_{uk}$ and $w = w_t$ and rearranging:

$$w_t = \frac{B}{\pi}\sqrt{4(\epsilon_{uk} + \alpha\Delta T)} \tag{27}$$

Table 1
EC2 ductility classes

Ductility class	ϵ_{uk} (%)
H	> 5
N	> 2.5

5.3. Calculation of stress–strain distribution due to combined loading

At the ultimate limit deflection w_t there will be tensile membrane forces throughout most of the slab and so some cracking of the concrete will occur. EC2 [22] states that for concrete in tension with cracks that Poisson's ratio should be taken as zero. In calculating the stress in the reinforcement at the deflection w_t it is therefore necessary to modify Eqs. (19) and (20) slightly to take account of this such that:

$$\sigma_{xx} = \frac{w_t^2 \pi^2 E_s}{8L^2}\left(1 - \cos\frac{2\pi y}{B}\right) - E_s \alpha \Delta T \tag{28}$$

$$\sigma_{yy} = \frac{w_t^2 \pi^2 E_s}{8B^2}\left(1 - \cos\frac{2\pi x}{L}\right) - E_s \alpha \Delta T \tag{29}$$

If the reinforcement bars are at a temperature that will cause the steel properties to degrade then appropriate reduced values of E_s and $\sigma_{y,T}$ should be chosen. The mechanical strains can be calculated using Eqs. (21) and (22). Again, a mechanical strain and mechanical stress should be calculated for every reinforcing bar and values of x and y should be chosen accordingly. The mechanical stress and mechanical strain at this deflection will be defined as σ_{w_t}, ϵ_{w_t}.

5.4. External work

Calculation of the external work done by the load is straightforward. Keeping the assumption that the deflected shape forms a double Fourier sine surface then the external work done is that of the load moving through the deflection w_q and can be calculated:

$$\Pi_{ext} = \int_0^L \int_0^B q_{ult} w_q \sin\frac{\pi x}{L} \sin\frac{\pi y}{B}\,dx\,dy = q_{ult} w_q \frac{4LB}{\pi^2} \tag{30}$$

5.5. Internal work

To determine the internal work done as the slab moves through the deflection w_q is a more complicated procedure. The internal work done must be calculated for every reinforcing bar as they are all different. Initially the stress strain states in the reinforcement caused by the thermal loading are considered. Due to the deflection w_T caused by the thermal load each bar will have a particular mechanical stress and strain σ_{w_T}, ϵ_{w_T}. These have been calculated in Section 4.5 using Eqs. (19)–(22).

If a square slab under thermal loading is considered then the largest deflections will occur at its centre. Fig. 10 shows a typical membrane stress distribution along the boundary of a laterally restrained slab with an aspect ratio close to one. It would be possible, however, for the membrane stresses at midspan to be compressive depending on the temperature distribution within the slab and the aspect ratio.

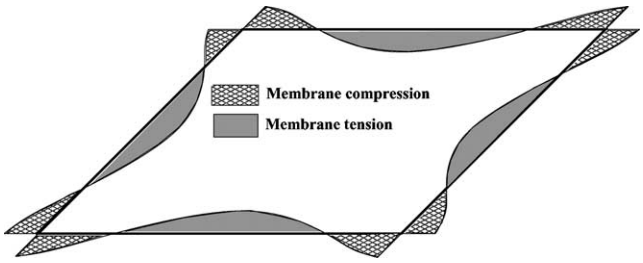

Fig. 10. Typical normal membrane stress distribution along slab boundary due to fire.

The failure point of the slab has been defined as when the slab has a total deflection of w_t corresponding to a limiting mechanical strain ϵ_{uk} in the reinforcement. Due to this deflection each reinforcing bar will have a mechanical stress and strain σ_{w_t}, ϵ_{w_t} as calculated in Section 5.3. At the deflection w_t the magnitude of the membrane stress distribution normal to the slab edge has changed. Fig. 11 shows the membrane stress distributions in the reinforcing bars along the boundary, the points represent the position of the reinforcing bars. It can be seen that more of the reinforcing bars are in tension under the combined loading. Near the middle of the slab boundary the reinforcing bars have reached yield such that $\sigma_{w_t} = \sigma_{y,T}$ and $\epsilon_{w_t} > \varepsilon_{y,T}$.

The internal work done is defined as the energy required to move from the stress–strain state σ_{w_T}, ϵ_{w_T} at a deflection of w_T due to the thermal loading to the stress–strain state σ_{w_t}, ϵ_{w_t} at a deflection of $w_t = w_T + w_q$ due to the combined loading. Fig. 12 shows a typical change in the stress–strain state for a reinforcing bar. The shaded area represents the internal work done.

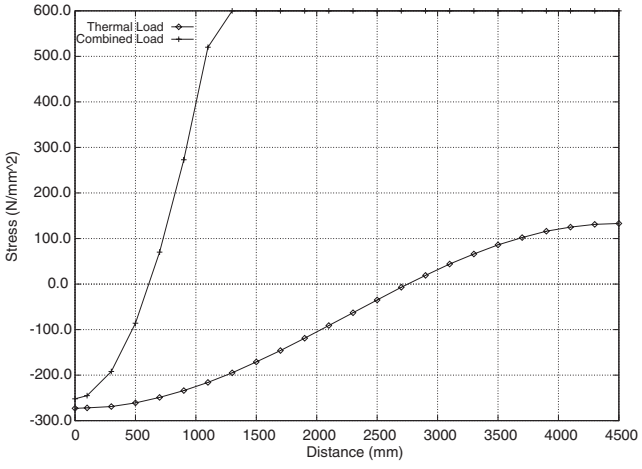

Fig. 11. Membrane stress in reinforcing mesh along slab boundary.

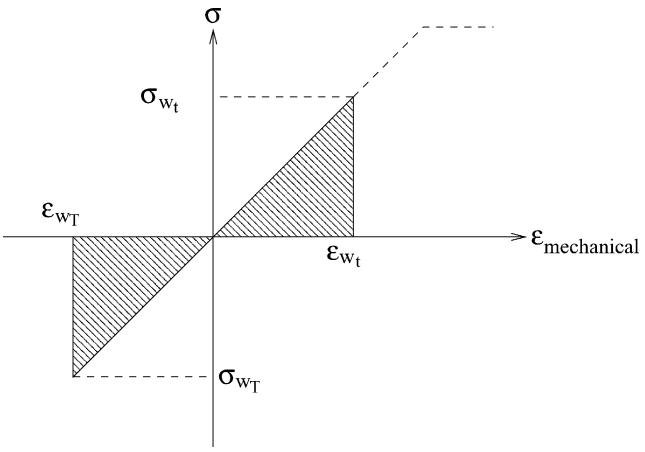

Fig. 12. Mechanical stress–strain in reinforcing bar.

Considering the differing stress–strain states in each reinforcing bar it can be seen that to calculate the internal work done is a complicated process. If V is the volume of a reinforcing bar then the total internal work done can be defined as:

$$\Pi_{\text{int}} = \sum_{n=1}^{\text{no. rebar}} \int^{V} \Delta\sigma\Delta\epsilon \, \mathrm{d}V \tag{31}$$

where

$$\Delta\sigma = \sigma_{w_t} - \sigma_{w_T} \tag{32}$$

$$\Delta\epsilon = \epsilon_{w_t} - \epsilon_{w_T} \tag{33}$$

Comparing the internal and external work done the ultimate load q_{ult} that the slab is capable of carrying can be calculated. The limit capacity that the slab is capable of carrying is given by:

$$q_{\text{ult}} = \frac{\Pi_{\text{int}}}{w_q \frac{4LB}{\pi^2}} \tag{34}$$

6. Design example

To illustrate the proposed new design method a 9 m × 9 m laterally restrained slab was analysed. A depth of 100 mm was assumed and reinforcement was taken to be a standard A142 mesh positioned at mid-height. The following material properties were assumed:

1. A yield strength of 600 N/mm^2 and a Young's modulus of 210,000 N/mm^2 were assumed for the mesh reinforcement.
2. A Young's modulus of $E = 40,000$ N/mm^2 was assumed for the concrete.

The slab was subjected to a Eurocode 1 parametric fire as described in Section 3.2. Two situations were considered; Load Case 1 has the highest thermal gradient at an earlier time in the fire scenario, while Load Case 2 has the highest thermal expansion at a later time (see Fig. 6). Both load cases were analysed using the method presented previously to determine their ultimate collapse load. The mesh reinforcement has a bar diameter of less than 16 mm so was considered to have normal ductility resulting in an ultimate mechanical strain limit of 2.5%. The results of the analysis are tabulated in Table 2.

Table 2
Results of two load cases for the design example

Load case	Time (s)	ΔT (°C)	$T_{,z}$ (°C)/mm	w_T (mm)	w_t (mm)	q_{ult} (kN/m^2)
1	3000	150	−6.1	252	927	6.91
2	4000	200	−5.0	282	934	7.09

Table 2 shows that the lowest capacity corresponds to Load Case 1 with an ultimate load of 6.91 kN/m^2. There is only a slight difference between the two load cases considered. Both of the calculated capacities were greater than a typical design load of 6.1 kN/m^2 for a slab of this size and geometry [10].

Bailey and Moore [9,10] analysed a slab with similar geometry and material properties using their proposed design method. They assumed a temperature difference of 770 °C between the top and bottom surfaces in the slab and a linear variation through the depth producing a thermal gradient of $T_{,z} = -7.5$ °C/mm. Thermal expansion was ignored as the slab was taken to be simply supported. They determined that the ultimate load capacity of the slab was 6.75 kN/m^2. This consisted of two components; the reduced bending strength of the exposed secondary beams and the membrane enhanced flexural capacity of the slab. Based on BS5950:Part8 [23] the load carrying capacity of the exposed secondary beams was 2.4 kN/m^2. The flexural capacity of the slab was calculated to be 1.21 kN/m^2, however, this was multiplied by an enhancement factor of 3.6 to produce a load capacity of 4.36 kN/m^2. The enhancement factor was calculated based on a limiting deflection of 460 mm. By combining the load capacity of the slab and the beams the total capacity of the system was calculated to be 6.75 kN/m^2 which was greater than the design load of 6.1 kN/m^2.

Although the method presented in this paper and that proposed by Bailey and Moore produce ultimate loads which are similar they are calculated from entirely different assumptions and rationale with regards to the behaviour of the slab. Therefore the similarity is probably a matter of chance. If the strength of the secondary beams are ignored then Bailey's method produces a slab capacity of 4.36 kN/m^2 at a limiting deflection of 460 mm. In comparison, using the method presented in this paper and based on the temperature distribution used by

Bailey the capacity of the slab at a limiting deflection of 460 mm is only 3.2 kN/m^2.

7. Conclusions

A new concept for assessment and design of reinforced concrete floor systems under fire has been presented. An ultimate limit state for fire loading has been proposed, on the basis of which a method to derive the ultimate capacity of the slab for any given fire has been presented. The method is based on the authors understanding of the most fundamental principles that govern the behaviour of composite structures in fire, and the output generated is fully consistent with these principles. Despite the rigorous nature of the background theory used, the authors believe that the method presented is reasonably straightforward and consistent with good engineering judgement and can potentially become a reliable engineering tool. However, there are a number of outstanding issues that must be addressed before this will be possible. These include further development issues, to cover a larger range of practical situations, such as, profiled concrete slabs and slabs composite with unprotected steel beams. But more importantly, there are fundamental issues, such as the assumption of material linearity with temperature (in the thermal deflection calculation), although there are good reasons why this may not be very significant. The greatest issue is the validation of the method, which can be achieved by comparing a number of sophisticated computational predictions and available experimental data. The computational validation work will begin soon as the most important next step, in order to establish that the method is both reliable and conservative.

One of the fundamental assumptions in the method is the availability of sufficient anchorage at boundaries. There are some important implications of this assumption with regards to the method presented, which are discussed below:

(1) Where fire compartments have discontinuous boundaries (no slab continuity), it is assumed that perimeter beams will provide the anchorage to the tensile membrane forces in the slab. This clearly occurred at Cardington (the explanation of the compressive ring action which does not rely upon lateral restraint is ignored as it has never been reliably quantified and would only assist the more direct lateral restraint assumption here). The authors assume that perimeter beams will be designed to resist the membrane anchorage forces obtained from the analysis here. These forces will exert inward 'pull' in the midspan regions of beams and 'outward push' near the ends, leading to significant torsional stresses in the transition regions, while reducing the requirement of the overall restraint. Given that no perimeter beam failures occurred at Cardington with no special design of this nature, it is reasonable to assume that if so designed a much more robust and predictable behaviour can be expected.

(2) The issue of strain localisation and consequent yield and rupture of reinforcement at the slab perimeters is the other contentious point. Such ruptures did occur in Cardington, but in very few locations on a very limited scale with practically no effect on overall structural stability. There is some argument about whether these cracks in the slabs occurred during heating or cooling. There is considerable evidence favouring the latter explanation (such as the lack of any heating damage on bags containing the loading sand near the cracks). There is however a much more compelling reason to believe this. Fig. 10 shows the typical distribution of membrane forces in a laterally restrained slab as a result of heating. It is clear that low deflections in the perimeter regions will induce compressions in the corners (as shown). When we look at the locations of the cracking in the Cardington tests, they are always near the corners (adjacent to columns). This is clearly incompatible with the membrane force distribution during heating. However when the slab begins to cool, considerable tensile strains are generated due to material contractions. One of the manifestations of this is seen in the very commonly occurring steel beam to column connections. It is very likely that the combined tensions generated along the perimeters during cooling (from the contracting steel beams and the slab) are sufficient to produce the few cracks in the slab seen in the Cardington tests. There are no such cracks in the midspan regions, where most of the tensile membrane action is anchored. The tensions in the perimeter regions during cooling are larger because these regions are likely to have experienced irrecoverable plastic strains during heating (unprotected steel beams experience very large plastic strains) leading to overall shortening of the members relative to original dimensions. This is less likely in the midspan regions where the thermal contractions during cooling may be accommodated in the recovery of deflection without any significant increase in membrane tension.

(3) The final question is that whether the slab capacity predicted using the method continues to be available during the cooling phase. This is perhaps the most difficult one to answer with the current state of knowledge. It can be said that for composite structures (steel frame with composite steel–concrete deck slabs), if one ensures the stability of steel beam column connections during cooling the capacity will increase as unprotected steel beams will regain strength and stiffness quickly. For reasonably massive concrete beams relatively undamaged by fire, similar assumptions can be made. The method is probably unsafe for concrete frames with flat slabs (or light concrete beams) as the capacity during cooling of such frames could reduce.

Acknowledgements

The authors are grateful to EPSRC and Ove Arup and Partners for the financial support for this work through an EPSRC Industrial CASE award.

References

[1] Structural fire engineering investigation of Broadgate phase 8 fire. Technical report, Steel Construction Institute, Ascot, UK, 1991.
[2] Martin DM, Moore DB. Introduction and background to the research programme and major fire tests at BRE Cardington. In: National Steel Construction Conference, May 1997. p. 37–64.
[3] Behaviour of steel framed structures under fire conditions. Technical Report Main Report, DETR-PIT Project, School of Civil and Environmental Engineering, University of Edinburgh, 2000. Available from: www.civ.ed.ac.uk/research/fire/project/technicalreports.html.
[4] Gillie M, Usmani AS, Rotter JM. A structural analysis of the first Cardington test. J Construct Steel Res 2001;57:581–601.
[5] Gillie M, Usmani AS, Rotter JM. A structural analysis of the Cardington British Steel Corner Test. J Construct Steel Res 2002;58:427–43.
[6] Lamont S, Usmani AS, Drysdale DD. Heat transfer analysis of the composite slab in the Cardington frame fire tests. Fire Safety J 2001;36:815–39.
[7] Usmani AS, Rotter JM, Lamont S, Sanad AM, Gillie M. Fundamental principles of structural behaviour under thermal effects. Fire Safety J 2001;36:721–44.
[8] Wang YC. Tensile membrane action in slabs and its application to the Cardington fire tests. Technical report, Building Research Establishment, 1996. Paper presented to the second Cardington Conference, 12–14 March 1996.
[9] Bailey CG, Moore DB. The structural behaviour of steel frames woth composite floor slabs subject to fire: *Part 1*: Theory. The Struct Eng 2000;78:19–27.
[10] Bailey CG, Moore DB. The structural behaviour of steel frames with composite floor slabs subject to fire: *Part 2*: Design. The Struct Eng 2000;78:28–33.
[11] Newman GM, Robinson JT, Bailey CG. Fire Safe Design: A new approach to multi-storey steel framed buildings. Technical report, Steel Construction Institute, Ascot, UK, 2000.
[12] Park R. Ultimate strength of rectangular concrete slabs under short term uniform loading with edges restrained against lateral movement. In: Proceedings of the Institution of Civil Engineers, vol. 28, May–August 1964. p. 125–50.
[13] Kemp KO. Yield of a square reinforced concrete slab on simple supports allowing for membrane force. The Struct Eng 1967;45(7):235–40.
[14] Lamont S. Behaviour of Steel Framed Structures in Fire. PhD thesis, University of Edinburgh, 1997. Available from: http://www.civ.ed.ac.uk/researc/fire/project/thesis.html.
[15] Eurocode 1: Basis of design and actions on structures. Technical Report ENV 1991-2-2, Brussels, European Committee for Standardisation, 1996.
[16] Carslaw HS, Jaeger JC. Conduction of heat in solids. Oxford: Clarendon Press; 1959.
[17] Huang HC, Usmani AS. Finite element analysis for heat transfer—theory and software. London: Springer-Verlag; 1994.
[18] Johnson RP, Buckby RJ. Composite structures of steel and concrete—vol. 2: Bridges. London, UK: Collins; 1986.
[19] Usmani AS, Lamont S. Key events in the structural response of a composite steel frame structure in fire. In: Proceedings of the SiF'02, The Second International Workshop for Structures in Fire, Christchurch, New Zealand, March 2002. p. 351–68.
[20] Johns DJ. Thermal stress analysis. Pergamon Press; 1965.
[21] Foray M, Newman M. The postbuckling analysis of heated rectangular plates. J Aerospace Sci 1962;29:1262, Technical note.
[22] Eurocode 2: Design of concrete structures. Technical Report ENV 1992-1-1, Brussels, European Committee for Standardisation, 1992.
[23] British Standard Institution. BS5950 Part 8: Code of Practice for Fire Resistant Design, 1990.